Article ID: 1000-7032(2010)04-0477-07

Impact of Asymmetry and Doping Density on Electron Raman Scattering in Triangular Double Quantum Wells

GU Dong-xia, LIU Cui-hong*, GUO Zheng-li, LU Fa
(*College of Physics and Electronic Engineering, Guangzhou University, Guangzhou* 510006, *China*)

Abstract: Electron Raman scattering (ERS) is investigated theoretically in asymmetric triangular double quantum wells (ATDQWs) within the framework of effective-mass approximation. The differential cross-section (DCS) is derived. Numerical calculations are performed for GaAs/$Al_xGa_{1-x}As$ ATDQWs. Results show that the ERS spectrum depends not only on the doping content but also on the asymmetry of ATDQWs. The spectrum yields a red shift with increasing the asymmetry of quantum wells or decreasing the Al doping content.

Key words: Raman scattering; double triangular quantum wells; intersubband transition; differential cross-section
CLC number: O472 **PACS:** 78.30.Fs **PACC:** 7830L **Document code:** A

1 Introduction

Recent developments in manufacturing technologies, such as molecular beam epitaxy and metal organic chemical vapor deposition, have made it possible to fabricate high quality semiconductor quantum structures with different shapes [1,2]. Owing to their unique electronic and optical properties, quantum-wells have attracted considerable attention in developing photoelectric devices, such as quantum well lasers, infrared detector and light modulators [3~7]. Due to the coupling effects in double quantum wells (DQWs), the single well energy states are split and the symmetry of the eigenstates can be reduced. This factor permits a variety of optical transitions which are forbidden in conventional single quantum wells to occur. If the distance between wells and the barrier in DQWs is changed, an improvement in the transport properties can be achieved. Thus, DQWs are more suitable than a single quantum well in technological applications. Since earlier experiments showed that the intersubband in a quantum well may have large dipole moment [8,9], intersubband transition within the conduction band of semiconductor quantum wells was widely studied from the viewpoints of both physical properties and novel device applications, and quantum wells photodetectors based on intersubband absorption were proposed to replace the conventional detectors [10,11]. Comparing with the rectangular quantum-well-structures light-emitting diodes (LEDs), the triangular quantum-well LEDs show a higher intensity, a lower operation voltage, a stronger light output power and a narrower linewidth of electroluminescence spectra [12]. Besides, triangular-shaped potentials were applied to enhance some special features of the electronic transport in the semiconductor heterostructures [13~15], and the liner, nonliner optical absorptions in asymmetric triangular double quantum wells (ATDQWs) were also studied [16].

Because of the precision in optical characterization of nanostructure research, Raman scattering has been used in theoretical and experimental investigations for low-dimensional semiconductor systems [17~21]. Considering different polarizations of incident and emitted radiation, the electronic structure of nano-

Received date: 2009-09-02; **Revised date:** 2009-11-13
Foundation item: Research supported by Natural Science Foundation of China(60878002).
Biography: GU Dong-xia, born in 1984, female, Shandong Province. Her work focuses on Raman scattering in low-dimensional system. E-mail: gudongxia1@163.com
*: Corresponding Author; E-mail: chliu64@yahoo.com.cn

structures can be thoroughly investigated[22,23]. Riera *et al.* studied the characteristic of rectangular DQWs[24]. Their research suggested that it was more efficient to use asymmetrical DQWs rather than asymmetrical triple quantum wells on building a tunable intersubband Raman laser. As far as we know, though the DQWs were studied widely, few people paid more attention to the influence of the system asymmetry on Raman scattering.

In this paper, the dependence of Raman shift on the well size and doping density are studied systemically in GaAs/$Al_xGa_{1-x}As$ ATDQWs. This paper is organized as follows:

In section 2, the energy spectrum and wave functions of the electrons in ATDQWs are provided. In section 3, the derivations of the DCS for the electron Raman scattering process is presented. In section 4, the numerical calculations and the discussion of results are performed. Finally, brief conclusions are given in section 5.

2 Model and Theory

We investigate the differential cross-section (DCS) in asymmetric double quantum wells with triangular potential. A schematic diagram of the AT-DQWs is shown in Fig. 1, in which z is the growth direction of this structure, V_0 is the height of the potential barrier, W_L and W_R represent the widths of the left-well and right-well, respectively.

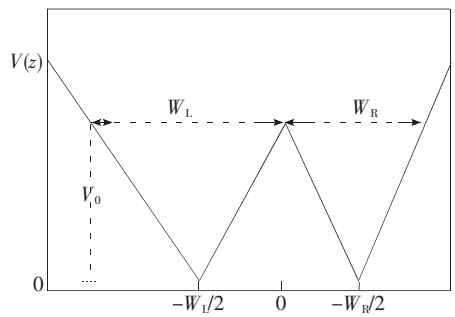

Fig. 1 Schematic diagram of ATDQWs

In the effective-mass approximation, the electron Hamiltonian and eigenstates can be written as[25]

$$H = -\frac{\hbar^2}{2m^*}\frac{d^2}{dz^2} + V(z), \tag{1}$$

where

$$V(z) = V_0\left|\frac{2z+W_L}{W_L}\right|\Theta(-z) + V_0\left|\frac{2z-W_R}{W_R}\right|\Theta(z), \tag{2}$$

and

$$\psi_{n_j}(z) = \begin{cases} c_{1,nj}Ai(\xi_{1,n_j}), & z \leqslant -W_L/2, \\ c_{2,nj}Ai(\xi_{2,nj}) + d_{2,nj}Bi(\xi_{2,nj}), & -W_L/2 \leqslant z \leqslant 0, \\ c_{3,nj}Ai(\xi_{3,nj}) + d_{3,nj}Bi(\xi_{3,nj}), & 0 \leqslant z \leqslant W_R/2, \\ c_{4,nj}Ai(\xi_{4,nj}), & z \geqslant W_R/2, \end{cases} \tag{3}$$

with

$$\xi_{1,nj,2,nj} = \alpha_{1,2}\left[\mp z - \frac{W_L}{2}\left(\frac{E_{nj}}{V_0} \pm 1\right)\right], \tag{4}$$

$$\xi_{3,nj,4,nj} = \alpha_{3,4}\left[\mp z - \frac{W_R}{2}\left(\frac{E_{nj}}{V_0} \mp 1\right)\right], \tag{5}$$

$$\alpha_{1,2} = \left[\frac{4m^* V_0}{W_L\hbar^2}\right]^{1/3}, \tag{6}$$

$$\alpha_{3,4} = \left[\frac{4m^* V_0}{W_R\hbar^2}\right]^{1/3}, \tag{7}$$

Here m^* is the effective mass of the conduction band, $\Theta(z)$ is the Heaviside step function, Ai and Bi are the regular and irregular Airy functions, and $n_j = 1, 2, 3, \cdots\cdots$ are the quantum numbers. The normalized coefficients $c_{1,nj}, c_{2,nj}, c_{3,nj}, c_{4,nj}, d_{2,nj}, d_{3,nj}$ and the eigenenergies E_{nj} can be numerically solved by the standard boundary condition of the electronic bound state[25].

3 Differential Cross-section

The DCS for electron Raman scattering of volume V per unit solid angle $d\Omega$ for incident light of frequency ω_l and scattering light of frequency ω_s is given by[19]

$$\frac{d^2\sigma}{d\omega_s d\Omega} = \frac{V^2\omega_s^2\eta(\omega_s)}{8\pi^3 c^4\eta(\omega_l)}W(\omega_s, \boldsymbol{e}_s), \tag{8}$$

where c is the velocity of light in vacuum, $\eta(\omega)$ is the refractive index as a function of the radiation frequency, $\boldsymbol{e}_s$ is the polarization vector of the emitted secondary radiation field, and $W(\omega_s, \boldsymbol{e}_s)$ is the transition rate calculated according to

$$W(\omega_s, \boldsymbol{e}_s) = \frac{2\pi}{\hbar}\sum_f |M|^2 \delta(E_f - E_i), \quad (9)$$

with

$$M = \sum_a \frac{\langle f|\hat{H}_s|a\rangle\langle a|\hat{H}_1|i\rangle}{E_i - E_a + i\Gamma_a} + \sum_b \frac{\langle f|\hat{H}_1|a\rangle\langle a|\hat{H}_s|i\rangle}{E_i - E_b + i\Gamma_b}, \quad (10)$$

where $|i\rangle$ and $|f\rangle$ denote the initial and final states of the system with their corresponding energies E_i and E_f, respectively. $|a\rangle$ and $|b\rangle$ are the intermediate states with energies E_a and E_b, respectively. Γ_a and Γ_b are the lifetime broadenings in the intermediate states.

The Hamiltonian operator $\hat{H}_1$ is

$$\hat{H}_1 = \frac{|e|}{m_0}\sqrt{\frac{2\pi\hbar}{V\omega_1}}(\boldsymbol{e}_1 \cdot \hat{\boldsymbol{P}}), \text{ with } \hat{\boldsymbol{P}} = -i\hbar\nabla, \quad (11)$$

where m_0 is the free electron mass. $\hat{H}_1$ describes the interaction between the electron and the incident radiation field in the dipole approximation. The interaction between the electron and the secondary radiation field is described by

$$\hat{H}_s = \frac{|e|}{m^*}\sqrt{\frac{2\pi\hbar}{V\omega_s}}(\boldsymbol{e}_s \cdot \hat{\boldsymbol{P}}), \quad (12)$$

It describes the photon emission by the electron after transitions between conduction subbands of the system.

By Eqs. (3), (11) and (12), we can obtain the following matrix elements

$$\langle\psi_{n3}|\hat{H}_1|\psi_{n1}\rangle = \frac{im^*|e|}{m_0}\sqrt{\frac{2\pi}{V\hbar\omega_1}}(E_{n3} - E_{n1}) \cdot \langle\psi_{n3}|\boldsymbol{e}_l \cdot z\boldsymbol{e}_z|\psi_{n1}\rangle = \frac{im^*|e|}{m_0}\sqrt{\frac{2\pi}{V\hbar\omega_1}}T_1, \quad (13)$$

and

$$\langle\psi_{n2}|\hat{H}_s|\psi_{n3}\rangle = i|e|\sqrt{\frac{2\pi}{V\hbar\omega_s}}(E_{n2} - E_{n3}) \cdot \langle\psi_{n2}|\boldsymbol{e}_s \cdot z\boldsymbol{e}_z|\psi_{n3}\rangle = i|e|\sqrt{\frac{2\pi}{V\hbar\omega_s}}T_2, \quad (14)$$

where

$$T_1 = (E_{n3} - E_{n1})\int_{-\infty}^{-\frac{W_L}{2}} c_{1,n3}Ai(\xi_{1,n3})(\boldsymbol{e}_1 \cdot z\boldsymbol{e}_z)c_{1,n1}Ai(\xi_{1,n1}) + \int_{-\frac{W_L}{2}}^{0}[c_{2,n3}Ai(\xi_{2,n3}) + d_{2,n3}Bi(\xi_{2,n3})](\boldsymbol{e}_1 \cdot z\boldsymbol{e}_z)[c_{2,n_1}Ai(\xi_{2,n1}) + d_{2,n1}Bi(\xi_{2,n1})] + \int_{0}^{\frac{W_R}{2}}[c_{3,n3}Ai(\xi_{3,n3}) + d_{3,n3}Bi(\xi_{3,n3})](\boldsymbol{e}_1 \cdot z\boldsymbol{e}_z)[c_{3,n_1}Ai(\xi_{3,n1}) + d_{3,n1}Bi(\xi_{3,n1})] + \int_{\frac{W_R}{2}}^{0}c_{4,n3}Ai(\xi_{4,n3})(\boldsymbol{e}_1 \cdot z\boldsymbol{e}_z)c_{4,n1}Ai(\xi_{4,n1}), \quad (15)$$

$$T_2 = (E_{n2} - E_{n3})\int_{-\infty}^{-\frac{W_L}{2}} c_{1,n2}Ai(\xi_{1,n2})(\boldsymbol{e}_s \cdot z\boldsymbol{e}_z)c_{1,n3}Ai(\xi_{1,n3}) + \int_{-\frac{W_L}{2}}^{0}[c_{2,n2}Ai(\xi_{2,n2}) + d_{2,n2}Bi(\xi_{2,n2})](\boldsymbol{e}_s \cdot z\boldsymbol{e}_z)[c_{2,n_3}Ai(\xi_{2,n3}) + d_{2,n3}Bi(\xi_{2,n3})] + \int_{0}^{\frac{W_R}{2}}[c_{3,n2}Ai(\xi_{3,n2}) + d_{3,n2}Bi(\xi_{3,n2})](\boldsymbol{e}_s \cdot z\boldsymbol{e}_z)[c_{3,n_3}Ai(\xi_{3,n3}) + d_{3,n3}Bi(\xi_{3,n3})] + \int_{\frac{W_R}{2}}^{0}c_{4,n2}Ai(\xi_{4,n2})(\boldsymbol{e}_3 \cdot z\boldsymbol{e}_z)c_{4,n3}Ai(\xi_{4,n3}). \quad (16)$$

In the initial state $|i\rangle$, we have an electron in the conduction band and one incident photon of energy $\hbar\omega_1$. The initial state energy is

$$E_i = \hbar\omega_1 + E_{n1}, \quad (17)$$

after the electron carries out a transition from the initial state to the intermediate state $|a\rangle$, the electron undergoes a transition toward the final state from the intermediate state, emitting the secondary radiation of energy $\hbar\omega_s$, thus,

$$E_f = \hbar\omega_s + E_{n2}, \quad (18)$$

By energy conservation law we get

$$E_i - E_a = E_{n2} - E_{n3} + \hbar\omega_s, \quad (19)$$

finally, we can write the DCS as

$$\frac{d^2\sigma}{d\omega_s d\Omega} = -\frac{e^4 m^{*2}\omega_s\eta(\omega_s)}{\hbar^3 c^4 m_0^2\omega_1\eta(\omega_1)}\frac{|T_1|^2|T_2|^2}{(E_i - E_a)^2 + \Gamma_a^2}, \quad (20)$$

4 Results and Discussion

In this section, the DCS of Raman scattering given by Eq. (20) is calculated numerically for $GaAs/Al_xGa_{1-x}As$ ATDQWs. The physical parameters are [26]:

$$m_b^* = 0.067m_0,\ m^* = m_b^* + 0.083x,$$

$$V_0 = 600(1.155x + 0.37x^2)\ \text{meV},$$

and $$\Gamma_a = \Gamma_b = 1\ \text{meV}.$$

From Eqs. (13) and (14), we can see that the transitions only occur when the polarization vector of the incident or emitted secondary radiation field is in the e_z direction. It can be seen from Eq. (19) that the emission spectra of the electronic Raman scattering show maxima when ω_s satisfies:

$$\omega_s = \frac{E_{n3} - E_{n2}}{\hbar}. \tag{21}$$

In Fig. 2, the effects of well sizes on the emission spectrum of the ATDQWs in the scattering configuration $X(Z,Z)\bar{X}$ are plotted. The right well widths we select here $W_R = 8, 9, 10, 11$ nm for Fig. 2 (a) and $W_R = 13, 14, 15$ and 16 nm for Fig. 2(b). The left-well width $W_L = 12$ nm and the doping content x in $GaAs/Al_xGa_{1-x}As$ quantum wells is kept at 0.35. On one hand, when $W_R < W_L$ in Fig. 2 (a), the position of the spectrum shifts to higher energy as W_R increases, which is similar to the rectangular DQWs [24], but is different from the rectangular double quantum wells, where the peak value of the emission spectrum diminishes with increasing the right-well widths in ATDQWs. On the other hand, the spectrum exhibits a red shift with increasing the width of right well in Fig. 2(b). The phenomenon can be explained by the asymmetry in ATDQWs. When the right well has the size of $W_R = 12$, *i. e.* $W_R = W_L$, the ATDQWs becomes a symmetric quantum wells. In Fig. 2, whether $W_R < W_L$ or $W_R > W_L$, the larger the difference between the right and left well is, the stronger the asymmetry is, and the resonant peaks suffer a red shift. In order to illustrate these phenomenon clearly, we plot Fig. 3, which presents the energy levels with increasing the various ratios of W_R and W_L.

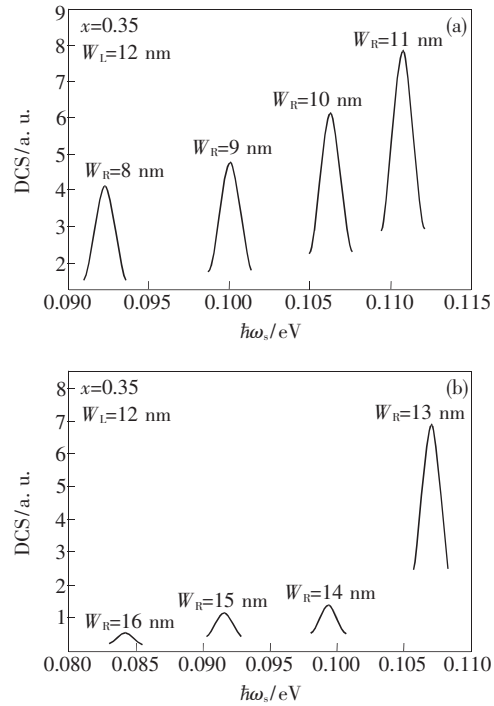

Fig. 2 Raman spectra of the $GaAs/Al_xGa_{1-x}As$ ATDQWs in the scattering configuration $X(Z,Z)\bar{X}$ with $x = 0.35$: (a) for $W_R < W_L$ and (b) for $W_R > W_L$; the sizes of the right-well $W_R = 8, 9, 10, 11, 13, 14, 15, 16$ nm and the left-well $W_L = 12$ nm.

Fig. 3 shows the energy-level of the electron as the function of the ratio W_R/W_L. This figure tells us that in the range of $\frac{W_R}{W_L} < 1$, the higher the W_R/W_L, the larger the energy-level differences between E_{n2} and E_{n3}. While, contrarily, in the range of $\frac{W_R}{W_L} > 1$,

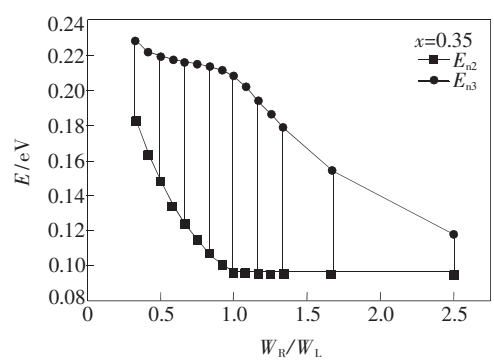

Fig. 3 The energy levels of electrons as a function of the ratios of W_R/W_L in the $GaAs/Al_xGa_{1-x}As$ ATDQWs with $x = 0.35$ in the scattering configuration $X(Z,Z)\bar{X}$. The vertical solid lines show the difference of the energy between E_{n2} and E_{n3}.

the higher the W_R/W_L, the smaller the energy-level differences between E_{n2} and E_{n3}. Namely, the asymmetry of the ATDQWs affcts sensitively the energy levels of the electron, which accords well with the Raman spectrum analyzed above.

In Fig. 4, we show the emission spectrum of the ATDQWs in the scattering configuration $X(Z,Z)\bar{X}$ with different Al doping content $x=0.3, 0.5, 0.8, 1.0$. The size of the left well and right well is kept at 12 nm and 9 nm, respectively. From this figure, we can see that, as x decreases from 1.0 to 0.3, the peak value increases and the spectrum shifts to lower energy, *i. e.* suffers a red shift. These observations are caused by alloying effects of the $Al_xGa_{1-x}As$ material [26,27]. The Al doping content x affects the effective mass of the electron and the height of the potential barrier V_0, which vary the difference of energy levels between electrons according to Eqs. (4) ~ (7).

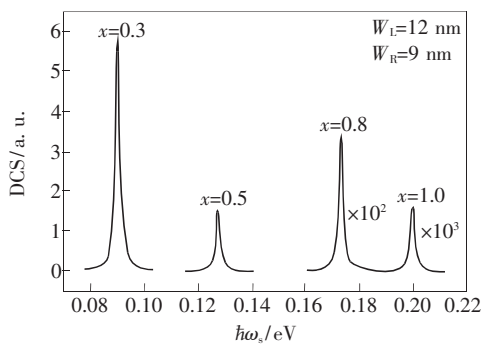

Fig. 4 Raman spectra of the $GaAs/Al_xGa_{1-x}As$ ATDQWs in the scattering configuration $X(Z,Z)\bar{X}$ with different Al doping content $x, x=0.3, 0.5, 0.8, 1.0$ with $W_L=12$ nm, $W_R=9$ nm.

5 Conclusion

In this work, we investigated theoretically the intersubband Raman scattering in ATDQWs in the effective-mass approximation. The explicit expressions of the DCS for intersubband electronic transition are derived. Numerical calculations are performed for ATDQWs with various difference of well widths and doping content in the scattering configuration $X(Z,Z)\bar{X}$. The results obtained show that the peak value and position of the spectrum are sensitively dependent on not only the Al doping content x, but also the asymmetry of quantum wells. When the difference of well widths between right and left well increased, the asymmetry of triangular double quantum wells is higher, and the displacement of the peaks toward low energy direction occurs, *i. e.* suffers a red shift. As x decreases, the displacement of the peaks appears a red shift. These behaviors of the $GaAs/Al_xGa_{1-x}As$ ATDQWs can be used in various optical device in infrared region.

References:

[1] Qian F, Li Y, Gradecak S, *et al*. Gallium nitride-based nanowire radial heterostructures for nanophotonics [J]. *Nano Letters*, 2004, **4**(10): 1975-1979.

[2] Li Zhixin, Wang Hongyan, Xin Wei, *et al*. Mean number of optical phonons of weak-coupling exciton in parabolic quantum dot [J]. *Chin. J. Lumin.* (**发光学报**), 2008, **29**(1): 1-4 (in English).

[3] Holonyak N, Kolbas R, Dupuis R, *et al*. Quantum-well heterostructure lasers [J]. *IEEE J. Quantum Electronics*, 1980, **16**(2): 170-186.

[4] Miller D A B. Quantum wells for optical information processing [J]. *Opt. Eng.*, 1987, **26**(5): 368-372.

[5] Weisbuch C, Nagle J. Quantum well semiconductor laser: US, 5081634 [P]. 1992-01-12. http://www.google.com/patents?hl=zh-CN&lr=&vid=USPAT5081634&id=ChchAAAAEBAJ&oi=fnd&dq=Quantum+well+semiconductor+laser&printsec=abstract#v=onepage&q=&f.

[6] Hofstetter D, Schad S S, Wu H, *et al*. GaN/AlN-based quantum-well infrared photodetector for 1.55 μm [J]. *Appl. Phys. Lett.*, 2003, **83**(3): 572-574.

[7] Wu Dianzhong, Wang Wenxin, Yang Chengliang, *et al*. InAs quantum dots with InGaAs caplayer infrared detector grown by MBE [J]. *Chin. J. Lumin.* (**发光学报**), 2009, **30**(2): 209-213 (in Chinese).

[8] West L C, Eglash S J. First observation of an extremely large-dipole infrared transition within the conduction band of a GaAs quantum well [J]. *Appl. Phys. Lett.*, 1985, **46**(12): 1156-1158.

[9] Levine B F, Malik R J, Walker J, *et al*. Strong 8.2 μm infrared intersubband absorption in doped GaAs/AlAs quantum well waveguides [J]. *Appl. Phys. Lett.*, 1987, **50**(5): 273-275.

[10] Coon D D, Karunasiri R P G. New mode of IR detection using quantum wells [J]. *Appl. Phys. Lett.*, 1984, **45**(6): 649-651.

[11] Pandey L N, George T F. Intersubband transitions in quantum well heterostructures with delta-doped barriers [J]. *Appl. Phys. Lett.*, 1992, **61**(9): 1081-1083.

[12] Choi R J, Hahn Y B, Shim H W, *et al*. Efficient blue light-emitting diodes with InGaN/GaN triangular shaped multiple quantum wells [J]. *Appl. Phys. Lett.*, 2003, **82**(17): 2764-2766.

[13] Lin F C, Chi W S, Huang Y S, *et al*. Piezoreflectance study of a GaAs/$Al_{0.23}Ga_{0.77}$As asymmetric triangular quantum well heterostructure [J]. *Semicond. Sci. Technol.*, 1995, **10**(7): 1009-1016.

[14] Kastalsky A, Peeters F M, Chan W K, *et al*. Novel nonlinear transport phenomena in a triangular quantum well [J]. *Semicond. Sci. Technol.*, 1992, **7**(3B): B530-B532.

[15] Nolle E L, Prokhorov A M. Efficient photoluminescence from triangular quantum wells at the interface of an InP/$In_{0.53}Ga_{0.47}$As heterostructure [J]. *JETP Lett.*, 1998, **67**(10): 826-831.

[16] Chen B, Guo K X, Wang R Z, *et al*. Liner and nonliner intersubband optical absorption in double trangular quantum wells [J]. *Solid State Commun.*, 2009, **149**(7-8): 310-314.

[17] Burnett J H, Cheong H M, Westervelt R M, *et al*. Resonant inelastic light scattering in remotely doped wide parabolic GaAs/Al_xGa_{1-x}As quantum wells [J]. *Phys. Rev.* B, 1993, **48**(7): 4524-4529.

[18] Zhao X F, Liu C H. Electron Raman scattering in cylindrical quantum wires [J]. *Eur. Phys. J.* B, 2006, **53**(2): 209-212.

[19] Bergues J M, Riera R, Comas F, *et al*. Electron Raman scattering in cylindrical quantum wires [J]. *J. Phys.: Condens. Matter*, 1995, **7**(36): 7273-7281.

[20] Zhong Q H, Liu C H. Well width-dependent electron Raman scattering in ZnS/CdSe cylindrical quantum dot quantum well [J]. *J. Raman Spectrosc.*, 2008, **39**(7): 953-958.

[21] Zhong Q H, Liu C H. Studies of electronic raman scattering in CdS/HgS cylindrical quantum dot quantum well structures [J]. *Thin Solid Film*, 2008, **516**(10): 3405-3410.

[22] Pinczuk A, Burstien E. *Light Scattering in Solids I* [M]. Edited by Cardona M, Heidelberg: Springer, Springer Topics in Applied Physics, 1983, 23.

[23] Cardona M. Lattice vibrations in semiconductor superlattices [J]. *Superlatt. Microstruct*, 1990, **7**(3): 183-192.

[24] Betancourt-Riera R, Rosas R, Marin-Enriquez I, *et al*. Electron Raman scattering in asymmetrical multiple quantum wells [J]. *J. Phys.: Condens. Matter*, 2005, **17**(28): 4451-4461.

[25] Santiago R B, Guimaraes L G. Extended eigenfunctions in asymmetric double triangular quantum wells in weak electric fields [J]. *Solid-State Electronics*, 2002, **46**(1): 89-96.

[26] Adachi S. GaAs, AlAs, and Al_xGa_{1-x}As material parameters for use in research and device applications [J]. *J. Appl. Phys.*, 1985, **58**(3): R1-R29.

[27] Mlayah A, Brugman A M, Carles R, *et al*. Surface phonons and alloying effects in $(CdS)_x(CdSe)_{1-x}$ nanospheres [J]. *Solid State Commun.*, 1994, **90**(9): 567-570.

双三角量子阱中不对称性及掺杂浓度对电子拉曼散射的影响

谷冬霞，刘翠红*，郭正丽，卢 发

（广州大学 物理与电子工程学院，广东 广州 510006）

摘要：在有效质量近似下，从理论上研究了非对称双三角量子阱的拉曼散射。推导了导带子带间电子跃迁

的微分散射截面表达式,以 $GaAs/Al_xGa_{1-x}As$ 材料为例进行了数值计算。结果表明,散射光谱不仅与掺杂浓度有关,而且与双量子阱的不对称性有关,随着量子阱不对称性的增加或掺杂浓度的减少,散射峰发生了红移。本工作对设计新型微电子和光电子器件有一定的指导意义。

关　键　词: 拉曼散射; 耦合三角量子阱; 子带间跃迁; 微分散射截面
中图分类号: O472　　**PACS:** 78.30.Fs　　**PACC:** 7830L　　**文献标识码:** A
文章编号: 1000-7032(2010)04-0477-07

收稿日期: 2009-09-02; **修订日期:** 2009-11-13
基金项目: 国家自然科学基金(60878002)资助项目
作者简介: 谷冬霞(1984 -),女,山东菏泽人,主要从事低维量子系统中的拉曼散射的研究。
E-mail: gudongxia1@163.com
*: 通讯联系人; E-mail: chliu64@yahoo.com.cn